Climate Dynamics (2020) 55:1443–1456
https://doi.org/10.1007/s00382-020-05330-2

Long-term trends in Arctic surface temperature and potential causality over the last 100 years

Haixia Xiao[1] · Feng Zhang[2] · Lijuan Miao[3,4] · X. San Liang[5] · Kun Wu[1] · Renqiang Liu[1]

Received: 25 August 2019 / Accepted: 11 June 2020 / Published online: 25 June 2020

Abstract
The rate of warming of the Arctic surface temperature has exceeded that of the global surface temperature in recent decades. However, the underlying process and causes of the long-term warming remain uncertain. In this paper, we explored the factors underlying variation in Arctic mean surface temperature anomalies (AMTA) using a piecewise linear model for 1920–2018. This analysis indicated that the change in AMTA during the study period could be divided into three segments, with AMTA increasing from 1920 to 1938, declining from 1939 to 1976, and finally increasing rapidly after 1977. By a newly developed rigorous formalism of information flow, we found a one-way causality from the driving forces to AMTA. Moreover, the AMTA evolution could mainly be attributed to a combined effect of anthropogenic and natural factors (e.g., CO_2, aerosol, and PDO). During the first warming stage (1920–1938), the PDO and aerosols are the main factors determining the change in AMTA. During the second warming stage (1977–2018), greenhouse gases, dominated by CO_2, are the major factors accounting for the Arctic warming. In 1939–1976, the observed cooling may be associated with aerosols, clouds, and land use. A better understanding of the driving mechanism underlying AMTA evolution provides insight into the historical Arctic climate change, and can improve the prediction of future changes in AMTA.

Keywords Arctic surface temperature · Segments · Causality · Driving force · Anthropogenic forcing

1 Introduction

The Arctic surface temperature has increased at more than twice the rate of the global average since 1979 (IPCC 2013). Amplified Arctic warming has contributed to a great extent to sustained global warming over the past decade (Huang et al. 2017). The increased Arctic temperature has diverse impacts on the atmosphere over the land and the sea, including melting glaciers and permafrost (Hubberten et al. 2013; Kargel et al. 2013), breaking the ice-sheet mass balance (Shepherd et al. 2012), decreasing sea ice extent (Stroeve and Notz 2018; Ding et al. 2019; Jahn 2019), reducing primary productivity over North America (Kim et al. 2017; Blackport et al. 2019), and affecting the global climate system by altering the ocean circulations and atmosphere (Smith et al. 2019). The Arctic will become even warmer in the next few decades, as predicted by simulations based on multiple climate models (IPCC 2014).

In fact, the Arctic surface temperature has exhibited different trends in different periods, particularly from the twentieth century. Many studies have focused on the cause of the mean temporal or spatial variation in Arctic temperature in recent years. Some studies have attributed the observed Arctic warming to human influence (Gillett et al. 2008), Atlantic Multi-decadal Oscillation (Chylek et al. 2009), or a combination of anthropogenic and natural causes (Jones et al. 2013). Najafi et al. (2015) demonstrated that the increase

✉ Feng Zhang
fengzhang@fudan.edu.cn

1 Collaborative Innovation Center On Forecast and Evaluation of Meteorological Disaster, Nanjing University of Information Science and Technology, Nanjing 210044, China

2 Department of Atmospheric and Oceanic Sciences and Institute of Atmospheric Sciences, Fudan University, Shanghai 200438, China

3 School of Geographical Sciences, Nanjing University of Information Science and Technology, Nanjing 210044, China

4 Leibniz Institute of Agricultural Development in Transition Economies (IAMO), 06120 Halle (Saale), Germany

5 Center for Ocean-Atmosphere Dynamical Studies, Nanjing University of Information Science and Technology, Nanjing 210044, China

in greenhouse gases has warmed the Arctic, and other anthropogenic forcings (mainly aerosols) have cooled the Arctic over the past century. Smith et al. (2019) systematically explain the causes of Arctic warming, including the changes in solar radiation, volcanic eruptions and anthropogenic aerosol emissions, decadal timescale variations in the Atlantic and Pacific sea surface temperatures, and so on. Moreover, numerous studies have shown that the Pacific Decadal Oscillation (Svendsen et al. 2018), black carbon (Shindell and Faluvegi 2009; Flanner 2013), orbital parameters (Crespin et al. 2013), as well as land use (Miao et al. 2016) contributed to climate change in the Arctic. However, the mechanisms underlying changes in Arctic mean surface temperature anomalies (AMTA) in particular periods remain unclear and controversial.

Several studies have analyzed the causes of the long-term evolution of the AMTA. One approach is the traditional statistical correlation analysis, but observed correlations do not necessarily imply causation (Sies 1988; Yang et al. 2016). Another approach is the optimal fingerprint method, which can be used to quantify the effects of external forces on temperature by statistical analysis based on a large amount of climate model data (Ribes et al. 2013). Shimizu et al. (2006) proposed a linear non-gaussian acyclic model for causal inference, but it is yet to be validated in real-world applications. Traditionally, the Granger causality test is a common statistical method for causal inference (Granger 1969). It has been used in previous studies (Triacca et al. 2013; Stern and Kaufmann 2014) of the causal relationship between radiative forcing and global temperature; these studies have shown that anthropogenic forcings cause variation in temperature, but the results are binary (yes or no), with much important quantitative information yet to be explored. Liang (2014) developed a novel and rigorous method that makes causal inference easy; it is based on information flow (IF), a real physical notion that is logically associated with causality and has recently been formulated ab initio (Liang 2008, 2016). This method can be used to quantitatively evaluate the two-way causal relationship between two-time series and to assess the importance of an individual driving force for temperature changes. It is worth mentioning that the IF formalism is rigorously established from first principles, rather than empirically defined as a hypothesis (ansatz), and, above all, the resulting formulas are very simple. It also should be mentioned that the IF formalism was originally developed for the atmosphere–ocean-climate science (e.g., the causal relation analysis between CO_2 and global warming by Stips et al. (2016), but so far has been successfully applied to other earth system sciences (e.g., Vannitsem et al. 2019), quantitative finance, neuroscience (Hristopulos et al. 2019), to name a few.

In this study, we aim to answer the two major questions. (1) What are the trends in AMTA from 1920 to 2018, and do any segments within this period exhibit different trends? (2) What is the causality between AMTA variation and various driving forces, and is the causality one-way or two-way? We believe that the answers to these questions will improve our understanding of the mechanism underlying the evolution of the Arctic temperature and increase our confidence in forecasting Arctic climate change.

2 Data

2.1 Arctic surface temperature datasets

Generally, Arctic surface temperature data lack either complete geographic coverage or field observations (Cowtan and Way 2014). To reduce the uncertainty of the AMTA, five temperature datasets were considered: the revision of HadCRUT by Cowtan and Way (2014), NASA GISTEMP (Hansen et al. 2010), HadCRUT4 (Morice et al. 2012), NOAA (Vose et al. 2012), and the reconstructed data by Huang et al. (2017) (hereafter H17). We specifically use the temperature anomalies (60°N–90°N) covering 1920–2018, and H17 data are from 1920 to 2014.

2.2 Driving force datasets

The annual global average radiative forcing data for 1920–2018 were applied in this study (https://www.pik-potsdam.de/~mmalte/rcps). This dataset includes annual data for (1) anthropogenic forcings, such as land use albedo (land use), total greenhouse gases (all-GHGs), CO_2, N_2O, total direct aerosol (aerosol), CH_4, and cloud albedo effect (cloud); and (2) natural forcings, including solar irradiance forcing (solar) and volcanic stratospheric aerosol forcing (volcanic).

The forcing datasets were derived from a combination of the Meinshausen historical data for the period from 1976 to 2005 (Meinshausen et al. 2011) and RCP4.5 for 2006–2018 (Representative Concentration Pathway in which radiative forcing is stabilized at approximately 4.5 W/m^2 per year after 2100). We know there is considerable uncertainty in both the solar and volcanic forcings (Suo et al. 2013). To address this issue, six total solar irradiance (TSI) datasets were used. They are the reconstructed TSI data by Lean (2000) [including the 11-year solar irradiance cycle (hereafter Lean1), plus the 11-year cycle with a background component (hereafter Lean2)], Lean and Rind (2008) (hereafter LR08), Crowley et al. (2003) (hereafter C03), Egorova et al. (2018) (hereafter E18), as well as data from https://lasp.colorado.edu/lisird/

data/historical_tsi/ [this data is reconstructed based on Wu et al. (2018) and Dudok de Wit et al. (2017), hereafter WD]. For time coverage, Lean1 and Lean2 are from 1920 to 2000, LR08 and WD from 1920 to 2018, C03 from 1920 to 1998, and E18 from 1920 to 2016.

Two natural internal modes that have been recognized as main drivers of climate variability over decadal time scales were also included, namely, Atlantic Multi-decadal Oscillation (AMO) and Pacific Decadal Oscillation (PDO) (Triacca et al. 2013). The time series of the monthly AMO index was obtained from the National Oceanic and Atmospheric Administration (NOAA) Earth System Research Laboratory's Physical Sciences Division (https://www.esrl.noaa.gov/psd/data/timeseries/AMO/), and the monthly PDO index was based on NOAA's reconstruction of SST (ERSST Version 4) (https://www.ncdc.noaa.gov/teleconnections/pdo/). The oceanic Atlantic meridional overturning circulation (AMOC) also affects the evolution of Arctic temperature. But we do not have its long-time record so far; it is hence not considered.

3 Methods

3.1 Segmenting the AMTA trend

A piecewise linear model was used to segment the trend in the AMTA from 1920 to 2018 in order to determine the years dividing segments and to characterize the trend in each stage (Liu et al. 2010). The main steps were as follows.

For a discrete time series containing T data points, consider a linear regression model of a structural change with m breakpoints (BPs) $T_1, T_2, \ldots, T_m$(m + 1 segments or regimes):

$$Y_t = \sum_{i=1}^{m+1} I_{\{T_{i-1}+1 \le t \le T_i\}}(a_i + b_i t) + N_t, \quad (t = 1, 2, \ldots, T) \quad (1)$$

where $T_0 = 0$, $T_m = T$, and I_A is an indicator variable that takes a value of 1 if event A is true and 0 otherwise. A continuity condition at each turning point is imposed: $a_i + b_i T_i = a_{i+1} + b_{i+1} T_i$. Y_t represents the observed dependent variable at time t, and a_i and $b_i (i = 1, 2, \ldots, m + 1)$ are trend regression coefficients for each segment. N_t is normally assumed to be autoregressive with a time lag of 1 or 2 (AR(1) or AR(2)), treated as an unexplained noise term.

The BPs $T_1, T_2, \ldots, T_m$ are treated as unknown. When T observations on Y_t are available, the first step is to estimate the unknown piecewise linear trend coefficients together with the positions of BPs. Supposing that N_t themselves can be regarded as independent random errors with mean zero and common variance δ_N^2, by the first- and second-order autoregressive models (AR(1) and AR(2)) as well as the model without autoregression (AR(0)), the noise term will be tentatively interpreted. Finally, the Monte Carlo method was used to estimate the uncertainties for all trend parameters (including the positions of BPs). To accurately estimate the standard deviations of the fitted trend parameters, 10,000 pseudorandom series were generated to simulate the corresponding normally distributed independent and identically distributed residuals.

The number of structural breaks m is unknown; it is estimated according to the least-squares principle. We assume it is known at the beginning, and then determine it by solving a model selection problem. The associated least-squares estimates of the coefficients for the trends in each m-partition T_1, $T_2, \ldots, T_m$ are calculated by minimizing the sum of squared residuals (Tomé and Miranda 2005):

$$S_T = \sum_{t=1}^{T} \left[Y_t - \sum_{i=1}^{m+1} I\{T_{i-1} \le t \le T_i\}(a_i + b_i t) \right]^2. \quad (2)$$

The estimated BPs $T_1, T_2, \ldots, T_m$ are such that $(\hat{T}_1, \hat{T}_2, \ldots, \hat{T}_m) = \arg\min_{T_1,\ldots,T_m} S_T(T_1, T_2, \ldots, T_m)$, satisfying the standard form of the Schwarz Bayesian information criterion (BIC) (Ng and Perron 2005; Portnyagin et al. 2006):

$$S_q = T \ln \left[\frac{1}{T} \sum_{t=1}^{T} (Y_t - \hat{Y}_t)^2 \right] + q \ln T. \quad (3)$$

In the above equation, $\hat{Y}_t$ is the modeled value (versus the residual) of the dependent variable at time t, and $q = 2m + 2$, $q = 2m + 3$, and $q = 2m + 4$ correspond to AR(0), AR(1), and AR(2), respectively. Those with the lowest and second-lowest BIC values were selected as the best and secondary models, respectively.

3.1.1 Interannual trend in AMTA over the last 100 years

Figure 1 shows that various datasets yield different values but similar trends. All of the datasets exhibit an increasing trend in the annual mean AMTA. The temperature anomalies from GISTEMP and Cowtan and Way are significantly higher than those from H17, while the values from NOAA are quite similar to the latter, and the those of HadCRUT4 lie in between. To reduce the uncertainty of AMTA, we take account into all the datasets by taking the average of them; that is to say, the annual AMTA hereafter is the mean of that from these datasets.

Figure 2 summarizes variation in annual AMTA from 1920 to 2018 and their corresponding trends based on different models with 0 to 5 BPs but without autoregression. Figure 3 shows the BIC values for different trend models applied to the time series of annual AMTA. The 2-BPs model with the lowest BIC value appeared to be the optimal

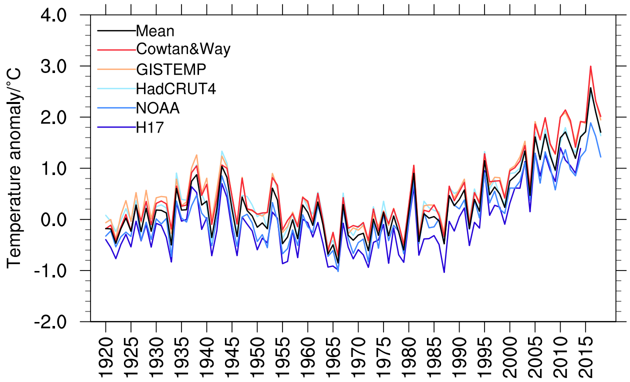

Fig. 1 Variation in the annual mean AMTA from 1920 to 2018. Datasets are from Cowtan and Way, GISTEMP, HadCRUT4, NOAA, and H17

choice (Figs. 2c, 3), while the 3-BPs model with the second-lowest BIC value was suboptimal (Figs. 2d and 3). Through Monte Carlo simulation, for the optimal piecewise result (Fig. 2c), the BP values were largely independent, reliable, and relatively stable, as the respective uncertainty intervals of these BPs had no overlap and were relatively small. Compared with the optimal 2-BPs model, the 0-BP and 1-BP models did not reproduce the cooling process. We hereafter evaluated the outputs of the 2-BPs model.

There are BPs in 1938 and 1976 according to the 2-BPs model. Based on this, the evolution of AMTA can be divided into three segments: (1) segment 1 (1920–1938), AMTA increased at a rate of 0.45 °C per decade; (2) segment 2 (1939–1976), AMTA declined with a relatively weak cooling trend of 0.18 °C per decade; (3) segment 3 (1977–2018), a warming trend was identified with a rate of increase of

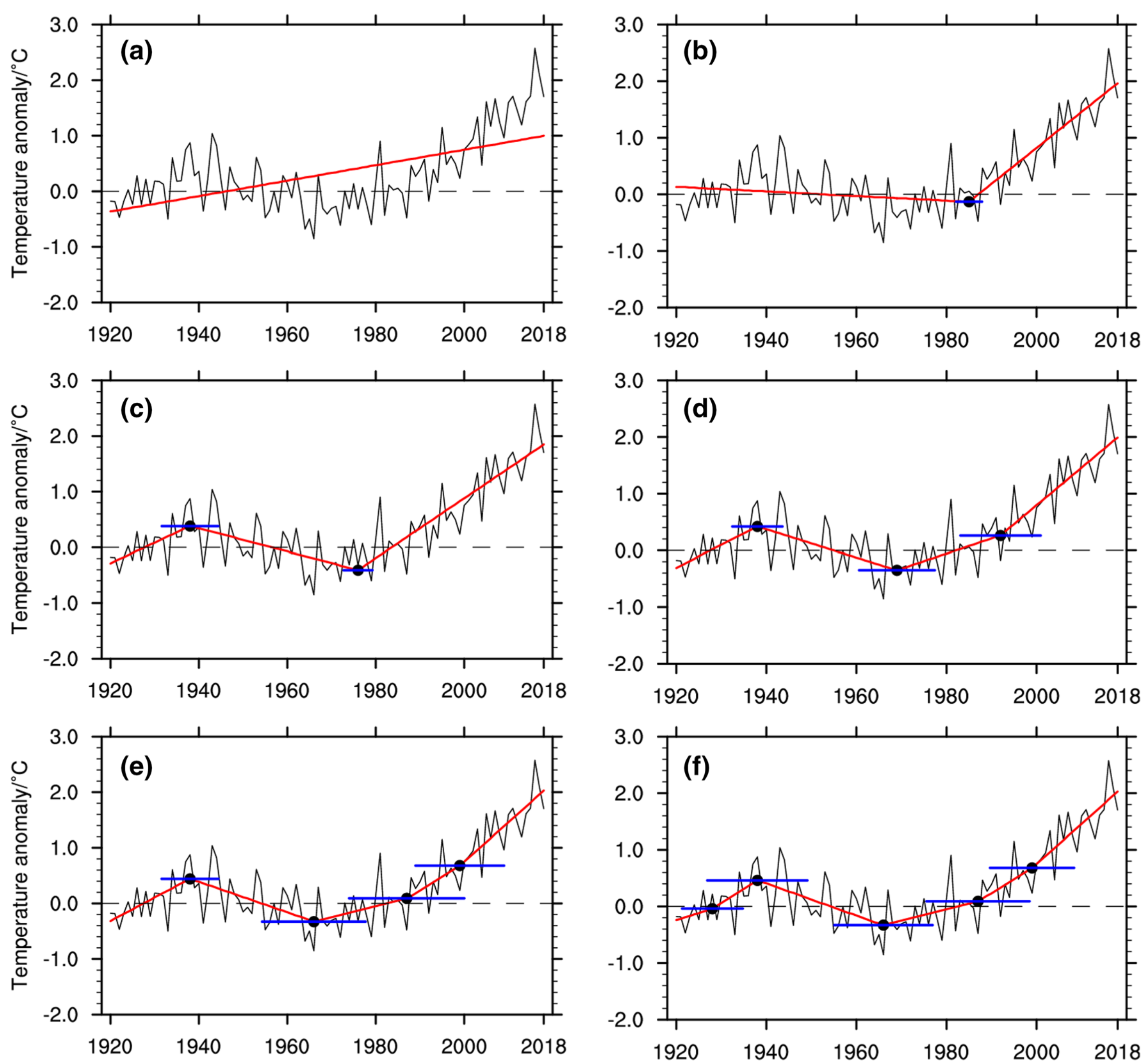

Fig. 2 Variation in annual AMTA from 1920 to 2018 (black solid line). The red solid line indicates the corresponding linear trend, (a)–(f) show results based on different BP models (0–5 BPs, without autoregression). Black dots plus blue error bars indicate the position(s) of the BPs and standard deviations

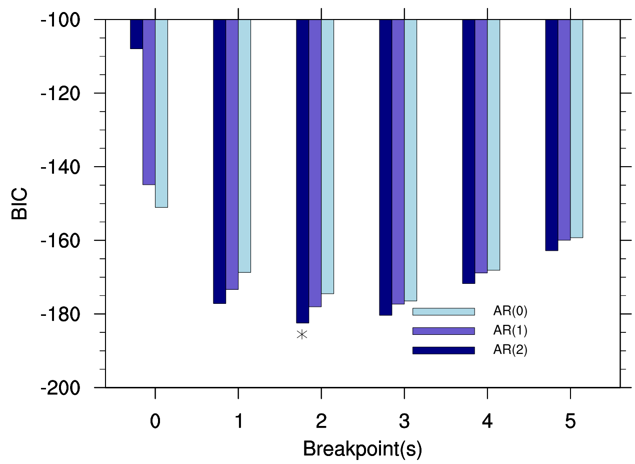

Fig. 3 BIC values for different linear models applied to the time series of annual AMTA. AR(0)/AR(1)/AR(2) indicates the corresponding autoregressive component. Note: "Asterisk" indicates the best model

0.54 °C per decade, much higher than that for segment 1. This indicates that AMTA increased rather rapidly, particularly after 1977.

3.2 Analysis of the causality between AMTA and driving forces

Causalities between the major driving forces and the AMTA time series were analyzed using the IF method. A detailed description is given in Liang (2014, 2016); the main steps are described here.

Given a two-dimensional nonlinear stochastic system with a vector field (F_1, F_2) and a matrix of stochastic perturbation amplitudes (b_{ij}), Liang proved that the rate of the information flowing from a component (say X_2) to another component (say X_1), denoted as $T_{2\to1}$ is, in a closed form,

$$T_{2\to1} = -E\left(\frac{1}{\rho_1}\frac{\partial(F_1\rho_1)}{\partial x_1}\right) + \frac{1}{2}E\left(\frac{1}{\rho_1}\frac{\partial^2(b_{11}^2 + b_{12}^2)\rho_1}{\partial x_1^2}\right) \quad (4)$$

(units: nats per unit time; simply referred to $T_{2\to1}$ as "information flow" or "flow" if no confusion arises), where E is the mathematical expectation, and ρ_1 is the marginal probability density of X_1. Equation (4) was first proved in 2008 (Liang 2008); refer to a recent comprehensive study (Liang 2016) for more details and, particularly, for multidimensional cases. Remarkably, Eq. (4) has the strict principle of causality, i.e., that an event evolves independently of another if it does not have causality from the latter, naturally embedded. $T_{2\to1}$ can be either zero or nonzero. A nonzero $T_{2\to1}$ means X_2 is causal to X_1, while a zero $T_{2\to1}$ means it is not.

When only two-time series X_1 and X_2 are given, $T_{2\to1}$ can be obtained through statistical estimation (the multivariate series case is referred to Liang, 2016). For linear systems Liang 2014 established that the maximum likelihood estimator (MLE) is very concisely expressed in the following form (units: nats per unit time):

$$T_{2\to1} = \frac{C_{11}C_{12}C_{2,d1} - C_{12}^2C_{1,d1}}{C_{11}^2C_{22} - C_{11}C_{12}^2} \quad (5)$$

where C_{ij} represents the sample covariance between X_i and X_j, and $C_{i,dj}$ is the covariance between X_i and $X_j = \left\{\frac{X_{j,n+1}-X_{j,n}}{\Delta t}\right\}$($\Delta t$ is the time step size). Note here we have abused the notation $T_{2\to1}$ for late convenience; here it is actually the MLE and hence should bear a hat. Ideally, if $\left|T_{2\to1}\right|$ is nonzero,X_2 is causal to X_1, and if not, X_2 is noncausal to X_1. However, in practice, statistical significance must be tested.

The above formula states that causality can be explicitly expressed as a combination of the sample covariance of the involved time series and their derivatives. Though with an assumption of linearity, it has been shown to be a good approximation for nonlinear time series, and it has been successfully validated with highly nonlinear touchstone systems that fail the classical causal inference techniques. However, when only two-time series X_1 and X_2 are considered (pairwise causality analysis), the results should be carefully justified, as indirect causality may be overlooked. Besides, in neglecting the variables other than the two under consideration, problems of spurious causality could arise. Fortunately, Liang (2018) established that the information flow between two parties is invariant upon arbitrary nonlinear transformation of the remaining parties (the 3rd and/or 4th, 5th,…). That is to say, although we may not know how the role of the hidden 3rd party may play, the information flow between the two parties under consideration is consistent, and hence the thus-inferred causality is relevant. Of course, the formula (5) is just the maximum likelihood estimator of the rigorously derived one (4), and hence the result may not be precise and must be justified.

A practical way is to perform statistical significance test, which is also made possible by Liang (2014) based on the observation that, for a large ensemble N, the maximum likelihood estimate of a parameter approximately obeys a normal distribution near its true value with a variance $\left(\frac{C_{12}}{C_{11}}\right)^2\hat{\sigma}_{a_{12}}^2$. Here $\hat{\sigma}_{a_{12}}^2$ is determined as follows: Calculate $I_{ij} = -\frac{1}{N}\sum_{n=1}^{N}\frac{\partial^2 \log\rho(\mathbf{X}_{n+1}|\mathbf{X}_n;\hat{\theta})}{\partial\theta_i\partial\theta_j}$ to form a Fisher information matrix $\mathbf{I}$. In the equation the conditional probability density function,

$$\rho(\mathbf{X}_{n+1} = \mathbf{x}_{n+1} | \mathbf{X}_n = \mathbf{x}_n) = \frac{1}{(2\pi) b_1 b_2 \sqrt{\Delta t}} e^{-\frac{1}{2}(\mathbf{x}_{n+1} - \mathbf{x}_n - \mathbf{f} - \mathbf{A}\mathbf{x}_n \Delta t)^T (\mathbf{B}\mathbf{B}^T \Delta t)^{-1} (\mathbf{x}_{n+1} - \mathbf{x}_n - \mathbf{f} - \mathbf{A}\mathbf{x}_n \Delta t)} \quad (6)$$

where Δt is the time stepsize, and $\mathbf{B} = \begin{pmatrix} b_1 & 0 \\ 0 & b_2 \end{pmatrix}$, $\mathbf{A} = \begin{pmatrix} a_{11} & a_{12} \\ a_{21} & a_{22} \end{pmatrix}$, $\mathbf{f} = \begin{pmatrix} f_1 \\ f_2 \end{pmatrix}$, include all the parameters. It is easy to show that the problem is decoupled (cf., Liang 2014). Here only those in the first row are needed, which we denote as for short:$\theta \equiv (f_1, a_{11}, a_{12}, b_1)$ (in the matrix they are evaluated with their corresponding MLEs). In statistics, it has been established that $(N\mathbf{I})^{-1}$ can be taken as the covariance matrix of $\hat{\theta}$ (see Liang 2014 for references), from which $\hat{\sigma}^2_{a_{12}}$ is picked out. Given a significance level, the confidence interval then can be found based on $\left(\frac{C_{12}}{C_{11}}\right)^2 \hat{\sigma}^2_{a_{12}}$. For example, given a level of 90%, then the confidence level of the estimated $T_{2\to 1}$ should be

$$\left[T_{2\to 1} - 1.65 \left(\frac{C_{12}}{C_{11}}\right)^2 \hat{\sigma}^2_{a_{12}}, \quad T_{2\to 1} + 1.65 \left(\frac{C_{12}}{C_{11}}\right)^2 \hat{\sigma}^2_{a_{12}} \right]. \quad (7)$$

Notice that, if the size of the ensemble is not large enough, the maximum likelihood estimate will be an under-representation of the true variance, which could lead to misleading conclusions about causality. In this study, the confidence intervals are all given at the 90% level. In principle, provided that the calculated information flow value is significantly different from zero (passes the significance test), a causal relationship then exists between the two-time series. But for the sake of safety, here we discard small absolute information flows (< 0.1 nat/ut) as insignificant, thanks to the quantitative nature of this novel causality analysis.

4 Results

4.1 Causal analysis between AMTA and the driving forces

We applied the IF method to explore the potential causality between multiple driving forces and AMTA (Table 1), specifically, All-GHGs, aerosol, CO_2, land use, and cloud are included in anthropogenic forces, and natural forces contain Solar, Volcanic, AMO, and PDO. Because the bold numbers indicate that the absolute IF was larger than 0.1 nat/ut and significant at the 90% confidence interval (that is, the absolute value of the IF is within the confidence interval); in this situation, there is a causal relationship between the driving forces and AMTA, and a greater IF means a greater causality. For the 0-BP model, the IF from anthropogenic forcing to AMTA is 0.332 ± 0.110 nat/ut and in the other direction is − 0.006 ± 0.003 nat/ut. It is clear that there is a one-way causality if the 0-BP model is considered, indicating that increased anthropogenic forcing is the main determinant of Arctic warming.

When applying the IF method to the best-fit 2-BPs model, the results are different from those of the 0-BP model.

Table 1 Information flow between driving forces (anthropogenic forces: all-GHGs, aerosol, CO_2, land use, and cloud; natural forces: solar, volcanic, AMO, and PDO) and AMTA variation

Driving forces	Forces → AMTA (nat/year)				AMTA → Forces (nat/year)			
Breakpoints	0-BP	2-BPs			0-BP	2-BPs		
Year	1920–2018	1920–1938	1939–1976	1977–2018	1920–2018	1920–1938	1939–1976	1977–2018
Total forcing	**0.389 ± 0.115**	**0.520 ± 0.173**	0.065 ± 0.058	**0.332 ± 0.177**	− 0.026 ± 0.063	0.000 ± 0.116	− 0.044 ± 0.039	0.021 ± 0.140
Antropogenic	**0.332 ± 0.110**	**0.419 ± 0.179**	0.058 ± 0.093	**0.874 ± 0.225**	− 0.006 ± 0.003	0.014 ± 0.019	0.008 ± 0.009	0.003 ± 0.010
All-GHGs	**0.246 ± 0.096**	**0.474 ± 0.187**	**0.171 ± 0.138**	**0.744 ± 0.220**	− 0.007 ± 0.001	0.002 ± 0.004	0.003 ± 0.003	0.002 ± 0.005
Aerosol	0.074 ± 0.054	**0.561 ± 0.224**	**0.233 ± 0.151**	0.019 ± 0.042	− 0.012 ± 0.003	− 0.046 ± 0.112	− 0.007 ± 0.011	− 0.037 ± 0.011
CO_2	**0.304 ± 0.106**	**0.470 ± 0.187**	**0.160 ± 0.134**	**0.892 ± 0.224**	− 0.006 ± 0.002	0.002 ± 0.006	0.006 ± 0.005	− 0.003 ± 0.006
Land use	**0.106 ± 0.065**	**0.263 ± 0.172**	**0.245 ± 0.150**	**0.194 ± 0.139**	− 0.003 ± 0.006	0.020 ± 0.038	0.018 ± 0.023	0.025 ± 0.029
Cloud	0.081 ± 0.057	**0.445 ± 0.204**	**0.234 ± 0.152**	**0.145 ± 0.117**	− 0.008 ± 0.002	− 0.007 ± 0.059	0.011 ± 0.008	− 0.038 ± 0.012
Solar	0.018 ± 0.022	**0.204 ± 0.162**	0.008 ± 0.041	− 0.000 ± 0.001	− 0.008 ± 0.016	0.080 ± 0.098	0.010 ± 0.026	0.001 ± 0.001
Volcanic	0.005 ± 0.015	0.028 ± 0.051	**0.171 ± 0.106**	0.060 ± 0.093	− 0.010 ± 0.014	− 0.021 ± 0.033	− 0.061 ± 0.074	− 0.032 ± 0.075
AMO	0.077 ± 0.070	**0.203 ± 0.183**	**0.128 ± 0.104**	**0.234 ± 0.193**	0.070 ± 0.069	0.095 ± 0.099	0.093 ± 0.089	0.155 ± 0.207
PDO	− 0.000 ± 0.002	**0.533 ± 0.366**	0.015 ± 0.034	0.031 ± 0.045	− 0.002 ± 0.003	− 0.079 ± 0.331	0.005 ± 0.032	0.063 ± 0.053

The unit time step is ut = 1 year. Causation significant at the 90% confidence level with an absolute IF larger than 0.1 nat/ut is shown in bold. The '± errors' represents the ± 90% confidence intervals

Figure 4 provides the annual radiative forcing from various factors and time series of AMO and PDO indices from 1920 to 2018. During the first warming period (segment 1: 1920–1938), we find a significant impact of changes in anthropogenic forcing (0.419 ± 0.179 nat/ut) on the Arctic temperature, of which CO_2 (0.470 ± 0.187 nat/ut), clouds (0.445 ± 0.204 nat/ut), and especially aerosols (0.561 ± 0.224 nat/ut) are the major contributors (Fig. 4 and Table 1). The changes in the radiative forcing of land use also contribute to AMTA. Besides, it is clear that enhanced PDO (0.533 ± 0.366 nat/ut) is the main factor determining the change in AMTA, and as the study shows that when PDO is transitioned to a positive phase, the deepening of the Aleutian Low and the poleward low-level advection of extratropical air warms the Arctic (Svendsen et al. 2018). Furthermore, our results show that AMO makes a contribution to Arctic warming, as it is the time of the transition of the AMO to its positive phase, with the possible transport of heat from the Atlantic Ocean to the Arctic Ocean. At the same time, the intensified solar irradiance is also a factor that caused Arctic warming, however, no significant impact of changes in volcanic forcing was detected, maybe due to a lull in volcanic activity (Table 1 and Fig. 4).

During the cooling period from 1939 to 1976 (segment 2), the cooling was mainly caused by aerosol (0.233 ± 0.151 nat/ut), cloud (0.234 ± 0.152 nat/ut), and land use albedo (0.245 ± 0.150 nat/ut). The radiative forcing by aerosols, clouds, and land use changes to a greater degree than in segment 1, indicating that as the radiative forcing decreases, the cooling effects decrease. Although All-GHGs, specifically CO_2 has a significant causal effect on AMTA, the contribution is negligible. Accordingly, a combined cooling effect

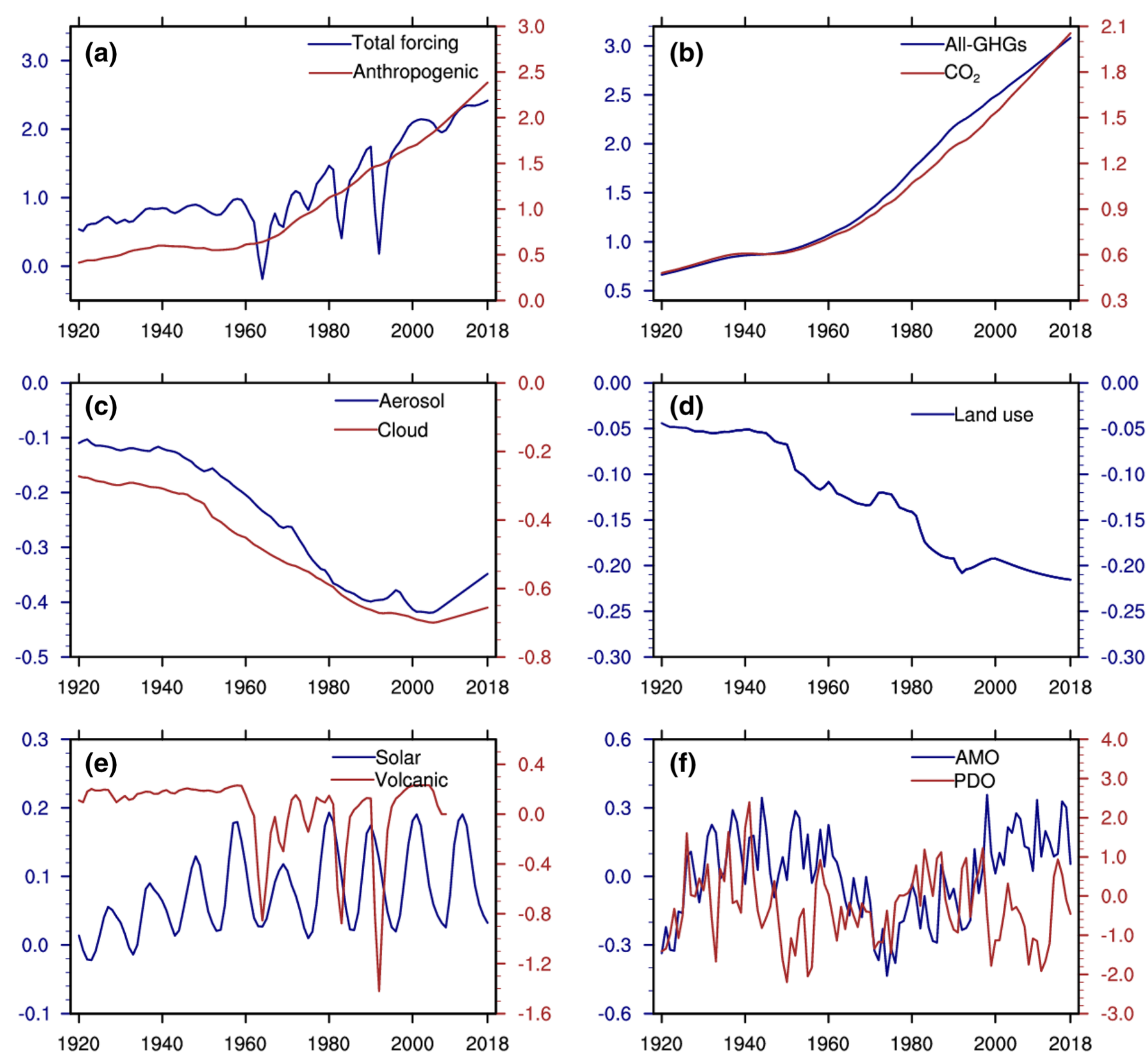

Fig. 4 Annual radiative forcing (W/m^2) change for various factors; time series of AMO and PDO indices cover 1920 to 2018. **a** Total forcing and anthropogenic forcing; **b** all-GHGs and CO_2; **c** aerosols and clouds; **d** land use; **e** natural radiative forcings: solar and volcanic; **f** AMO and PDO indices

overwhelmed the CO_2 warming impact in this period. Additionally, volcanic forcing and AMO also contribute to Arctic cooling, and this may be explained by the same volcanic eruptions (e.g., the volcanic eruption on Agung in 1963) and transition of the AMO to its negative phase (the heat transported from the Atlantic to the Arctic Ocean might be reduced) (Fig. 4).

During the second warming period from 1977 to 2018 (segment 3), Arctic warming was largely driven by the increase in all-GHGs (0.744 ± 0.220 nat/ut), particularly CO_2 (0.892 ± 0.224 nat/ut). It is worth noting that their IF values were larger than that for segment 1, explaining the rapid warming in the Arctic during this period. Other anthropogenic forcings, including clouds and land use, are also responsible for the warming, but the contribution to Arctic warming is small, owing to the low values of radiative forcing. Moreover, AMO made a small contribution, and this corresponded to the time of the transition of the AMO to its positive phase, as in segment 1.

Since the IFs from AMTA to driving forces are negligibly small (Table 1), and combining the results of the above analysis, the driving forces we evaluated here exhibit a one-way causality (i.e., there was a causal effect from driving forces to Arctic warming but not from the Arctic warming to driving forces).

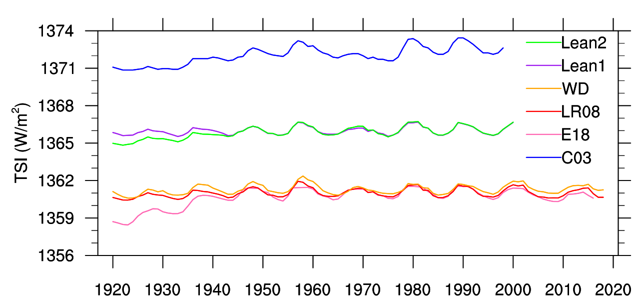

Fig. 5 Annual radiative forcing (W/m^2) change for diverse TSI

Considering that large uncertainty exists in solar forcing data, especially in those for the early twentieth century, and we can only take into account different increments of TSI to present different variants of possibilities. The TSI data we used are just as mentioned in Sect. 2. Whereas the solar irradiance (Fig. 4) is changed from 1920 to 1938 by only ca. 0.11 W/m^2, the change in various TST (Fig. 5) during 1920–1938 ranges around ca. 0.26 W/m^2 (Lean1), 0.74 W/m^2 (Lean2), 0.48 W/m^2 (LR08), 0.55 W/m^2 (WD), 0.91 W/m^2 (C03) and 2.37 W/m^2 (E18). The IFs between these different TSI's and AMTA are listed in Table 2. From it we see that, from 1920 to 1938, overall, TSI is indeed a factor driving Aritic warming, though not the main factor (for comparison, note that the information flow value from the contemporary PDO is 0.533 ± 0.366 ut/nat). The results with Lean1 and C03 are similar to those in Table 1. The results with LR08 (0.337 ± 0.198 ut/nat), WD (0.318 ± 0.222 ut/nat), and especially Lean2 (0.409 ± 0.179 ut/nat), all show an increased responsibility of TSI for Arctic warming. The IF from TSI to AMTA based on E18, which is 0.056 ± 0.091 nat/ut and hence insignificant, is, however, significant during segment 2 (1939–1976). This indicates that the IF does not always increase as solar irradiance increases; in other words, the amount of change in TSI maybe not the factor determining the IF value. Actually, as shown in Fig. 5, there exists obvious differences between these diverse TSI data, but we cannot evaluate which one is more representative at the present stage of our knowledge. Since the time series of TSI has a large uncertainty, the results may also be uncertain. Moreover, the time span, which contains 19 years (1920–1938), is not long enough for statistical analysis, and hence may account for part of the uncertainty in the results. For all these reasons, it is not our intension to make conclusive statements based on these results; they should be just taken as a reference for future work.

To see which regions of the Arctic are most sensitive to the driving forces or where the driving forces contribute significantly to the changes in temperature, we apply the

Table 2 Information flow between TSI and AMTA variation

TSI	TSI → AMTA (nat/year)				AMTA → TSI (nat/year)			
Breakpoints	0-BP	2-BPs			0-BP	2-BPs		
Year	1920–2018	1920–1938	1939–1976	1977–2018	1920–2018	1920–1938	1939–1976	1977–2018
Lean1		**0.201 ± 0.174**	− 0.005 ± 0.048			0.087 ± 0.115	0.011 ± 0.032	
Lean2		**0.409 ± 0.179**	0.019 ± 0.066			0.082 ± 0.112	0.016 ± 0.044	
LR08	0.000 ± 0.000	**0.337 ± 0.198**	0.001 ± 0.046	− 0.003 ± 0.033	− 0.000 ± 0.000	0.107 ± 0.127	0.014 ± 0.029	0.032 ± 0.029
WD	0.014 ± 0.019	**0.318 ± 0.222**	0.000 ± 0.001	0.005 ± 0.009	− 0.002 ± 0.016	0.096 ± 0.147	− 0.000 ± 0.001	− 0.005 ± 0.008
C03		**0.204 ± 0.181**	− 0.003 ± 0.032			0.099 ± 0.117	0.006 ± 0.020	
E18 (1920–2016)	0.009 ± 0.027	0.056 ± 0.091	**0.176 ± 0.106**	0.017 ± 0.076	− 0.014 ± 0.025	− 0.058 ± 0.061	− 0.051 ± 0.076	− 0.003 ± 0.076

The unit time step is ut = 1 year. Causation significant at the 90% confidence level with an absolute IF larger than 0.1 nat/ut is shown in bold. The '± errors' represent the ± 90% confidence intervals same causality analysis to the Arctic-gridded AMTA. Due to the sparse observations of historical temperature in the Arctic, we use the reconstructed data H17 for 1920–2014, which have an improved temporal and spatial coverage, to represent the Arctic air surface temperature and the associated dynamic processes (Huang et al. 2017).

Figure 6 shows that the effects of anthropogenic forcings on Arctic warming are mainly caused by greenhouse gases dominated by CO_2. In segment 1, significant IFs for CO_2 are detected over the Arctic Ocean, Norwegian Sea, Greenland Sea, north of Greenland, Baffin Island, and Baffin Sea; in particular, the Norwegian Sea has the most significant causality (Fig. 6g). The regions with significant IFs for aerosols and clouds are similar to those for CO_2 (Fig. 7); however, the regions with significant-high causality for land use are over Iceland. In segment 2, significant IFs for CO_2 are detected over Northeastern Canada and Greenland. For aerosols, land use, and clouds, the significant IFs are found over the Barents Sea and Northern Siberia (Fig. 7b, e, h). In segment 3, for CO_2, in addition to Alaska, Western Siberia, and Central Siberia, there are significant IFs in other parts of the Arctic, and in Ellesmere Island and the Greenland Sea as well. Regions with significant causality for aerosols, land use, and clouds are also observed over Eastern Greenland, Northern Russia, and Scandinavia (Fig. 7c, f, i).

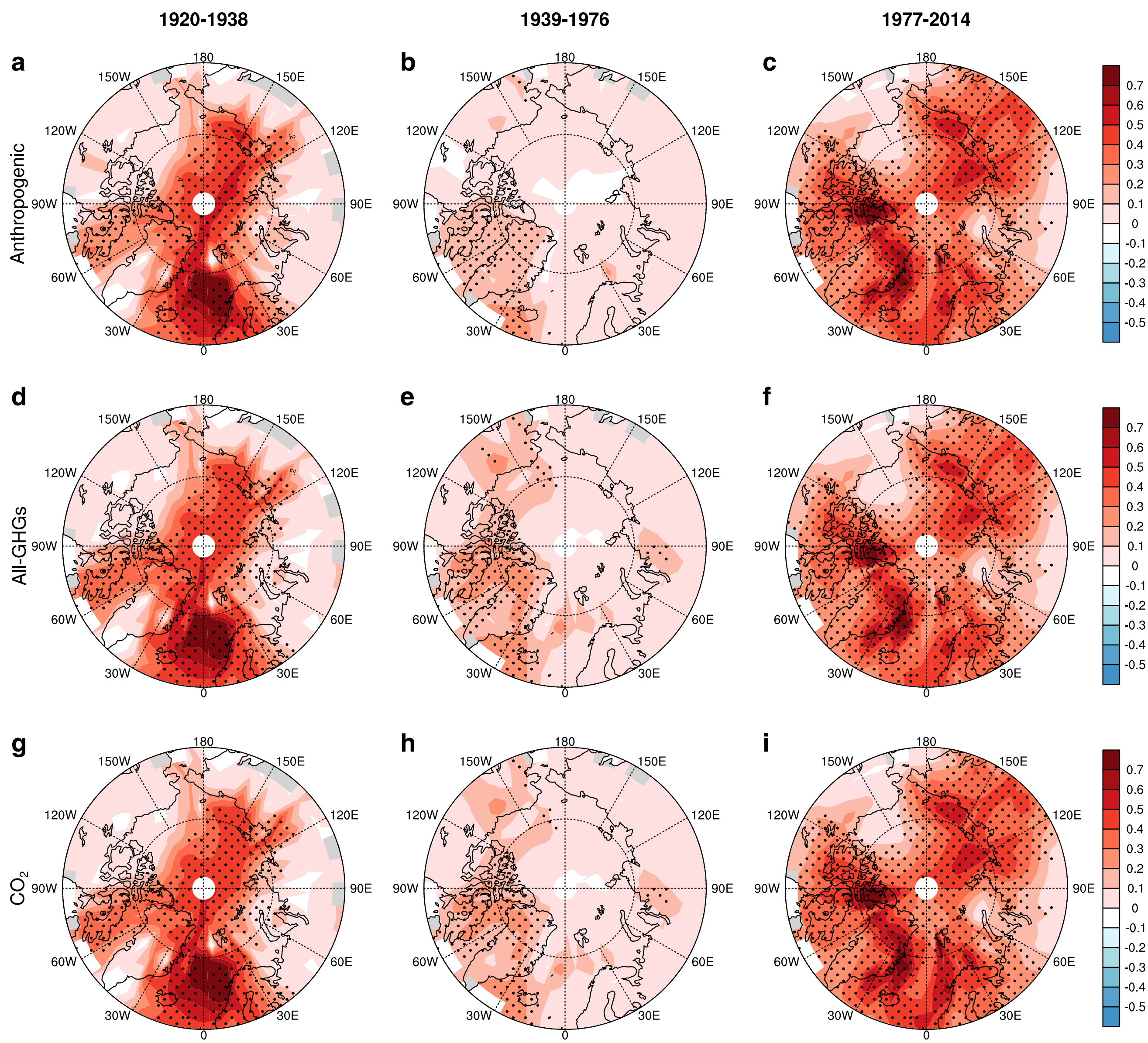

Fig. 6 Spatial distributions of the information flows from anthropogenic forcings to the gridded AMTA (H17) during different periods. The stippling represents significant causation at the 90% confidence level with absolute IF larger than 0.1 nat/ut

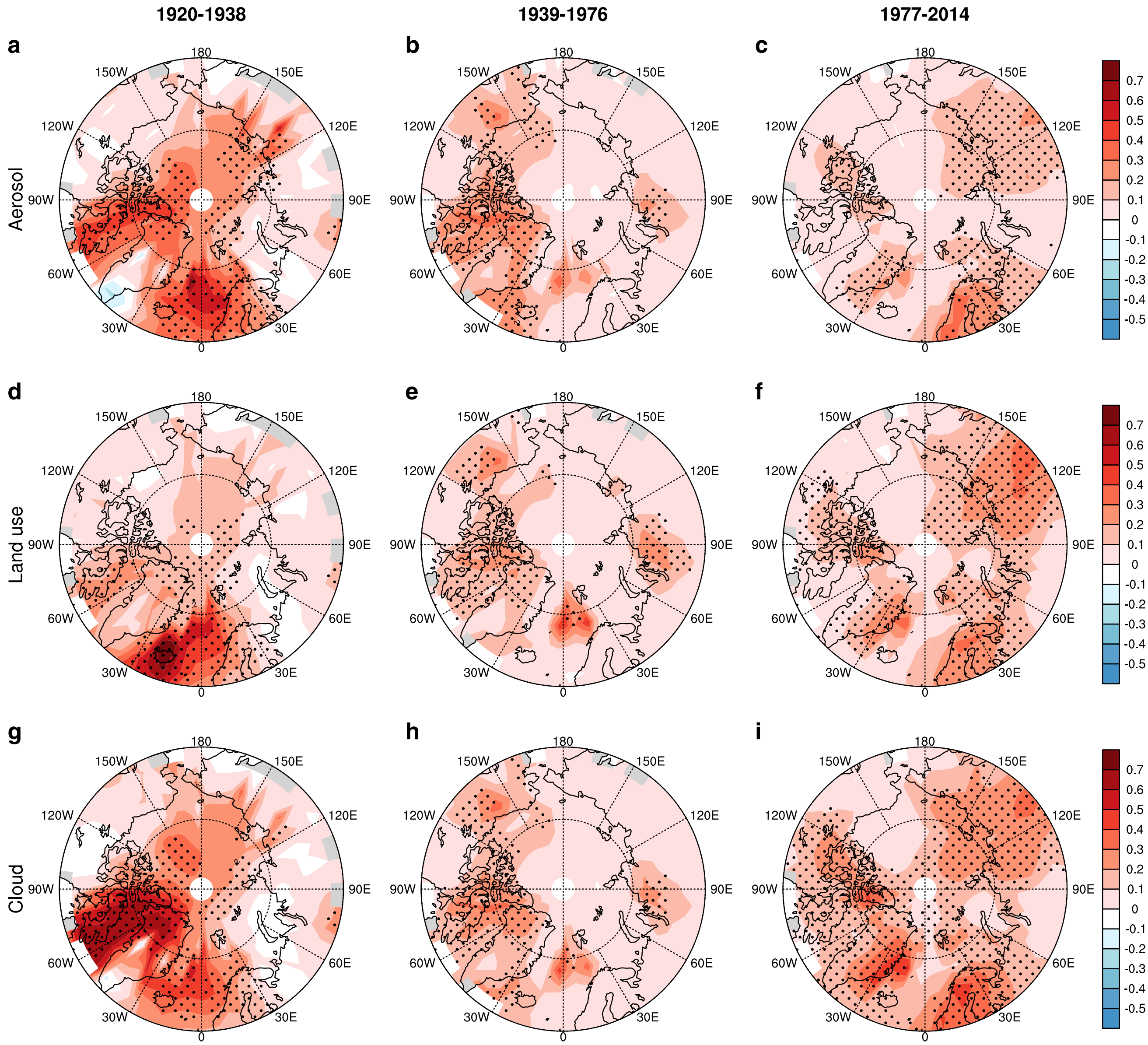

Fig. 7 Spatial distributions of the information flows from other anthropogenic forcings to the gridded AMTA (H17) during different periods. The stippling represents significant causation at the 90% confidence level with absolute IF larger than 0.1 nat/ut

The causalities from the natural forcings reveal different scenarios (Fig. 8a–f). The spatial distribution of the IF from the solar forcing to AMTA shows that during the considered period, the flow is only significant in segment 1, consistent with the previous analysis (Table 1), and the regions with significant causality are in northeastern Canada and Greenland. For the causality from volcanic forcing to AMTA, we can see that in segment 1, over the Arctic it is basically insignificant; in segment 2, there are significant IFs over Ellesmere Island and the Eastern Siberian Sea; in segment 3, the significant IFs are over the Baffin Sea and Western Greenland.

For internal climate modes, the causal scenario also differs. From the spatial distribution of the IF from AMO to AMTA (Fig. 8g, h, i), several regions with significant causality are identified in the Arctic. In segment 1, the IF value is significant over the North Atlantic, providing an additional first-order validation of the method when applied to climate data. In segments 2 and 3, the IFs are significant mainly over Northeastern Canada and Greenland. The most significant causality appears in segment 3, agreeing with the previous analysis based on Arctic mean values. For PDO, (Fig. 8j, k, l), the IF from it to AMTA is insignificant in segments 1 and 2. Besides, in segment 3 it is significant over the Central Arctic Ocean and the Eastern Siberian Sea and its coastal

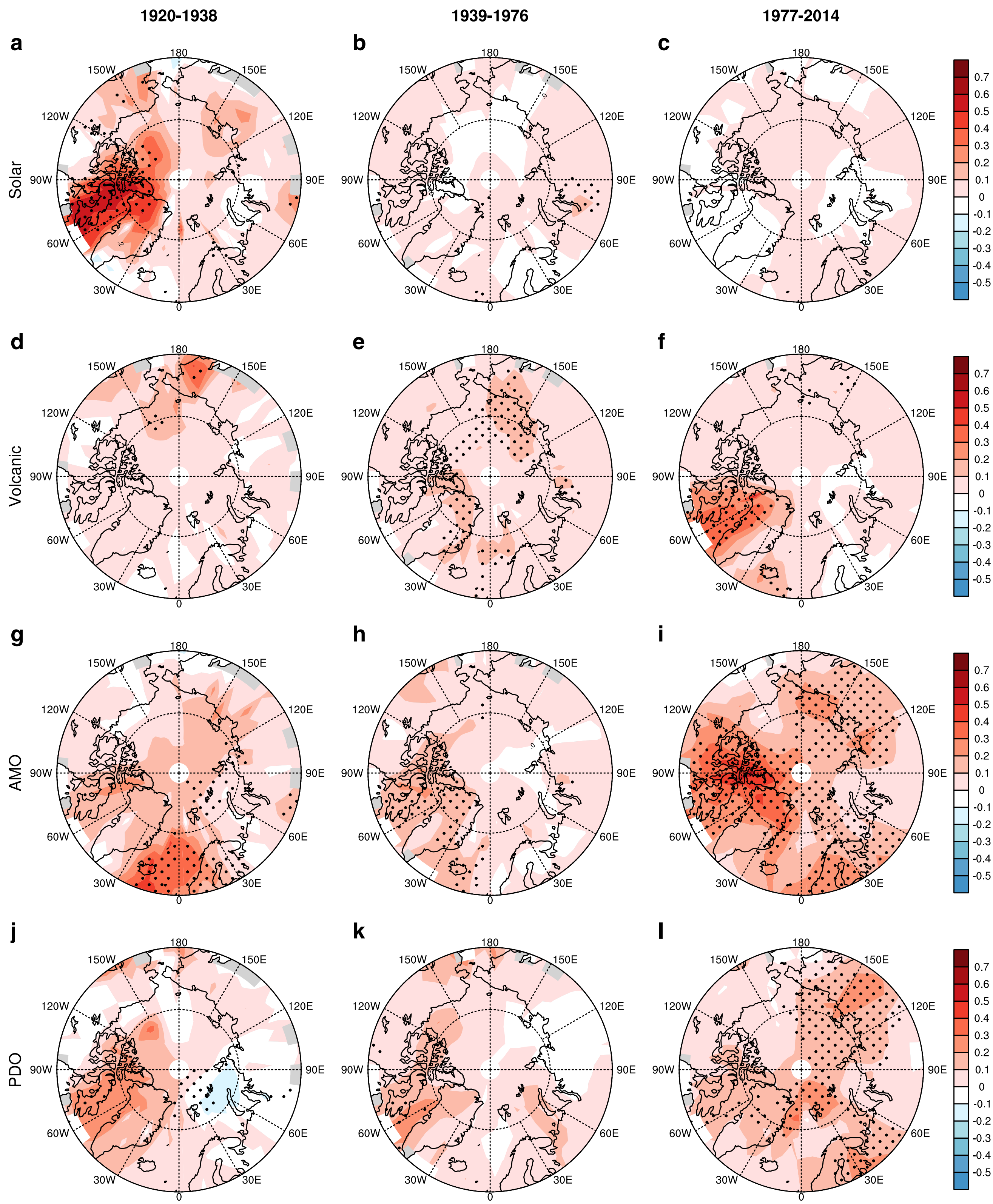

Fig. 8 Spatial distributions of the information flows from natural forcings and natural internal modes to the gridded AMTA (H17) during different periods. The stippling represents significant causation at the 90% confidence level with absolute IF larger than 0.1 nat/ut

areas. This may be due to the transition of the PDO first to its negative phase and then a recent shift to the positive PDO phase (Screen and Francis 2016) in segments 3, with the gradually deepened Aleutian Low, which contributes to the advection of warm and moist air into the central Arctic, and consequently further warms the Arctic. It's worth mentioning that when we apply the same causality analysis to the Arctic-gridded AMTA, the reconstructed data we used is H17, which is different from the average AMTA data when doing causality analysis of average AMTA. Because the data used are not completely consistent, therefore, in segment 1 (1920–1938), the results do not show the effect of PDO on the spatial distribution of AMTA, which are not completely consistent with the results in Table 1. Besides, Arctic surface temperature data was sparse (Cowtan and Way 2014; Dodd et al. 2015) especially in the early twentieth century because it lacks continuous and detailed observations, and the spatial distribution of the Arctic temperature data was estimated by interpolation approaches (Huang et al. 2017), which would inevitably have some errors. Overall, we think the causality results from average AMTA data are relatively reasonable and representative, and spatial results by using reconstructed data H17 can be used as a reference, but more precise results need to be verified by using more reliable AMTA data and simulated with climate models in the future.

5 Discussion and conclusions

Arctic warming's attribution is one of the most controversial issues in climate research. One reason for these controversies is that the method which people usually use is numerical simulation. Although numerical modeling is, in principle, the dynamically sound way to causal inference, models themselves may result in quite uncertain outcomes; for example, different models may have different physical parameterizations which will yield quite different results. For this reason, it is somehow difficult to reach a persuasive conclusion based only on modeling/simulation results. And, for the same reason, data-driven inference based solely on observations provides an alternative approach, and this has been a common practice in climate research, as can be evidenced in the numerous studies based on, say, correlation analyses. In this study, we followed the same tradition, doing a thorough investigation of causality analysis, using the state-of-the-art approach, namely, the recently rigorously established information flow (IF) analysis. We want to remark that, the method we are using is physically sound; that is to say, it is originated from real physics, not statistics. So, besides the attribution, the computed result has its physical meaning.

Applying a piecewise linear model, we found that there were three distinct segments for the trend in reconstructed Arctic surface air temperature. That is, two warming periods from 1920 to 1938 and 1977 to 2018 and a cooling period in between from 1939 to 1976 were detected. Our results are consistent with those of previous studies, such as Chylek et al. (2009), Fyfe et al. (2013), Johannessen et al. (2016), and Suo et al. (2013), who discovered that the Arctic temperature increased from the early twentieth century to 1939/1940, decreased from 1940 to 1969/1970, and increased again from 1970 to the late twentieth century. Our cooling period is slightly longer (1939–1977), and the second warming period is later than that reported in other studies. Additionally, a study has shown that recent and sustained warming began in the 1980s (ACIA 2005). However, Przybylak and Wyszyński (2020) proposed that warming was not seen until the mid-1990s by investigating the changes in Arctic temperature from 1951 to 2015. This may be due to the coverage of their study area, which is slightly different from ours–They used data from 37 meteorological stations that contain the area north of 60°N. In contrast to Chylek et al. (2009), who found that the warming rate in the Arctic was more rapid in 1910–1940 than in 1970–2008, our results showed that the former is slower, better reflecting recent observations.

Based on the IF results as computed, from 1920 to 1938, the long-term AMTA variation can be largely explained by local responses to PDO, aerosols, and other anthropogenic forcings (e.g., CO_2 and cloud). Previously, Fyfe et al. (2013) showed that the observed Arctic warming was likely owing to the rising black carbon aerosol emissions and the transition of the AMO to its positive phase (Fyfe et al. 2013); this is consistent with our results on AMO. Suo et al. (2013) argued that much of the Arctic warming in the early twentieth century could be explained by intensified solar radiation and a lull in volcanic activity during the 1920s to 1950s. Our results support this argument. From 1939 to 1976, aerosols, land use, and clouds are the main contributors to the temperature decline, and the contribution of greenhouse gases dominated by CO_2 to Arctic warming is small, though the emission of CO_2 does not decrease during this period. That is to say, during this period, aerosols, land use, and clouds offset the effect of warming caused by CO_2. However, given the small IF values and the slow changes in AMTA during this period, the internal climate variability may also affect the Arctic temperature change. Indeed, we detected a significant effect of change in AMO on AMTA, in agreement with previous studies such as (Chylek et al. 2009; Johannessen et al. 2016), and so forth. During the warming period in recent years (since 1977), the long-term Arctic temperature variation is dominated by the influence of all-GHGs, and CO_2 in particular. This substantiates once again the observation that Arctic warming is mainly GHG warming (Fyfe et al. 2013).

To summarize, we applied a piecewise linear regression model to explore the long-term trends in the AMTA in 1920–2018 to detect climate trends and their structural changes in time series based on the principle of least squares, with a priori unknown breakpoints. The best piecewise linear model is a 2-BPs trend model that divides the evolution of AMTA into three distinct segments by the years 1938 and 1976. We quantitatively estimated the causal relation between driving forces and AMTA using a recently developed rigorous formalism of IF. By calculating the IF value of each driving force to AMTA for each segment in the 2-BPs model, we found that the main drivers of the AMTA trend are both from anthropogenic and some natural forcings. Overall, there is one-way causation from driving forces to Arctic warming. We also found that CO_2 is the main contributor to Arctic warming. The impacts of CO_2 and other anthropogenic forcings (aerosols, cloud, and land use) and natural forcings (PDO and AMO) on the Arctic are important, and need to be taken into account when addressing and predicting future climate change in the Arctic.

We remark that, although we segmented the evolution of AMTA, there are still some uncertainties about the segmentation; that is to say, the length of each period may vary slightly. We discussed the driving forces associated with each period, but the set of driving forces is far from complete. Other drivers may exist. Also, the period of 1920–1938, which contains 19 years, is not long enough for statistical analysis. That is to say, the ensemble is small, inevitably leading to uncertainty in the results. Considering this, our results just provide a reference for the Arctic warming investigation. Moreover, because the causal relationship depends on the temperature data and forcing data, the uncertainties of temperature and forcing data result in the uncertain causalities. Besides, it lacks long time recond of the forcings such as AMOC, which prevents us from making a complete causal inference with all the identified climate modes. Further verification with, say climate model experiments are needed in future studies.

Acknowledgements The authors thank the National Oceanographic and Atmospheric Administration (NOAA) for providing the AMO and PDO data, and the Potsdam Institute for Climate Impact Research, Germany, for providing the driving forces dataset. Special thanks also go to Huang et al. for proving the Arctic temperature. The authors also would like to thank the anonymous reviewers and editors for their insightful comments and suggestions, which have significantly improved this paper. This study was financially supported by the National Natural Science Foundation of China (41675003, 41775008, and 41575040).

References

ACIA (2005) Arctic climate impact assessment. Cambridge University Press, Cambridge. https://doi.org/10.1007/978-3-319-25582-8_10037

Blackport R, Screen JA, van der Wiel K, Bintanja R (2019) Minimal influence of reduced Arctic sea ice on coincident cold winters in mid-latitudes. Nat Clim Change 9:697–704. https://doi.org/10.1038/s41558-019-0551-4

Chylek P, Folland CK, Lesins G, Dubey MK, Wang M (2009) Arctic air temperature change amplification and the Atlantic Multidecadal Oscillation. Geophys Res Lett 36:61–65. https://doi.org/10.1029/2009GL038777

Cowtan K, Way RG (2014) Coverage bias in the HadCRUT4 temperature series and its impact on recent temperature trends. Q J R Meteorol Soc 140:1935–1944. https://doi.org/10.1002/qj.2297

Crespin E, Goosse H, Fichefet T, Mairesse A, Sallaz-Damaz Y (2013) Arctic climate over the past millennium: annual and seasonal responses to external forcings. Holocene 23:321–329. https://doi.org/10.1177/0959683612463095

Crowley TJ, Baum SK, Kim K-Y et al (2003) Modeling ocean heat content changes during the last millennium. Geophys Res Lett 30:1932. https://doi.org/10.1029/2003gl017801

Ding QH, Schweiger A, L'Heureux M et al (2019) Fingerprints of internal drivers of Arctic sea ice loss in observations and model simulations. Nat Geosci 12:28–33. https://doi.org/10.1038/s41561-018-0256-8

Dodd E, Merchant CJ, Rayner NA, Morice CP (2015) An investigation into the impact of using various techniques to estimate Arctic surface air temperature anomalies. J Clim 28:1743–1763. https://doi.org/10.1175/jcli-d-14-00250.1

Dudok de Wit T, Kopp G, Fröhlich C et al (2017) Methodology to create a new total solar irradiance record: making a composite out of multiple data records. Geophys Res Lett 44:1196–1203. https://doi.org/10.1002/2016GL071866

Egorova T, Schmutz W, Rozanov E et al (2018) Revised historical solar irradiance forcing. Astron Astrophys 615:A85. https://doi.org/10.1051/0004-6361/201731199

Flanner MG (2013) Arctic climate sensitivity to local black carbon. J Geophys Res Atmos 118:1840–1851. https://doi.org/10.1002/jgrd.50176

Fyfe JC, Salzen KV, Gillett NP, Arora VK, Flato GM, Mcconnell JR (2013) One hundred years of Arctic surface temperature variation due to anthropogenic influence. Sci Rep 3:2645. https://doi.org/10.1038/srep02645

Gillett NP, Stone DA, Stott PA et al (2008) Attribution of polar warming to human influence. J Geophys Res Atmos 1:750–754. https://doi.org/10.1038/ngeo338

Granger CWJ (1969) Investigating causal relations by econometric models and cross-spectral methods. Econometrica 37:424–438

Hansen J, Ruedy R, Sato M, Lo K (2010) Global surface temperature change. Rev Geophys 48:1–29. https://doi.org/10.1029/2010RG000345

Hristopulos D, Babul A, Babul SA, Brucar LR, Virji-Babul N (2019) Disrupted information flow in resting-state in adolescents with sports related concussion. Front Hum Neurosci 13:419. https://doi.org/10.1101/671685

Huang JB, Zhang XD, Zhang QY et al (2017) Recently amplified arctic warming has contributed to a continual global warming trend. Nat Clim Change 7:875. https://doi.org/10.1038/s41558-017-0009-5

Hubberten HW, Boike J, Lantuit H (2013) Arctic warming and its consequences for Permafrost. Paper presented at the ISAR-3 (Third International Symposium on the Arctic Research), Tokyo, Japan

IPCC (2013) Climate change 2013: the physical science basis. In: Stocker TF et al (eds) Working Group I contribution to the Fifth assessment report of the Intergovernmental Panel on Climate Change. Cambridge University Press, Cambridge

IPCC (2014) Climate Change 2014: Synthesis Report. In: Core Writing Team, Pachauri RK, Meyer LA (eds) Contribution of Working

Groups I, II and III to the Fifth Assessment Report of the Intergovernmental Panel on Climate Change. IPCC, Geneva

Jahn A (2019) Reduced probability of ice-free summers for 1.5 degrees C compared to 2 degrees C warming. Nat Clim Change 9:726–726. https://doi.org/10.1038/s41558-019-0569-7

Johannessen OM, Kuzmina SI, Bobylev LP et al (2016) Surface air temperature variability and trends in the Arctic: new amplification assessment and regionalisation. Tellus A 68:28234. https://doi.org/10.3402/tellusa.v68.28234

Jones GS, Stott PA, Christidis N (2013) Attribution of observed historical near-surface temperature variations to anthropogenic and natural causes using CMIP5 simulations. J Geophys Res Atmos 118:4001–4024. https://doi.org/10.1002/jgrd.50239

Kargel J, Bush A, Leonard G (2013) Arctic warming and sea ice diminution herald changing glacier and cryospheric hazard regimes. In: EGU general assembly conference abstracts, vol 15, p 14188

Kim JS, Kug JS, Jeong SJ et al (2017) Reduced North American terrestrial primary productivity linked to anomalous Arctic warming. Nat Geosci 10:572–576. https://doi.org/10.1038/NGEO2986

Lean J (2000) Evolution of the Sun's spectral irradiance since the Maunder Minimu. Geophys Res Lett 27:2425–2428. https://doi.org/10.1029/2000GL000043

Lean JL, Rind DH (2008) How natural and anthropogenic influences alter global and regional surface temperatures: 1889 to 2006. Geophys Res Lett 35:L18701. https://doi.org/10.1029/2008GL034864

Liang XS (2008) Information flow within stochastic dynamical systems. Phys Rev E Stat Nonlinear Soft Matter Phys 78:031113. https://doi.org/10.1103/PhysRevE.78.031113

Liang XS (2014) Unraveling the cause-effect relation between time series. Phys Rev E Stat Nonlinear Soft Matter Phys 90:052150. https://doi.org/10.1103/PhysRevE.90.052150

Liang XS (2016) Information flow and causality as rigorous notions ab initio. Phys Rev E 94:052201. https://doi.org/10.1103/PhysRevE.94.052201

Liang XS (2018) Causation and information flow with respect to relative entropy. Chaos 28:075311. https://doi.org/10.1063/1.5010253

Liu RQ, Jacobi C, Hoffmann P, Stober G, Merzlyakov EG (2010) A piecewise linear model for detecting climatic trends and their structural changes with application to mesosphere/lower thermosphere winds over Collm, Germany. J Geophys Res Atmos 115:D22105. https://doi.org/10.1029/2010JD014080

Meinshausen M, Smith SJ, Calvin K et al (2011) The RCP greenhouse gas concentrations and their extensions from 1765 to 2300. Clim Change 109:213–241. https://doi.org/10.1007/s10584-011-0156-z

Miao LJ, Zhu F, Sun ZL, Moore JC, Cui XF (2016) China's land-use changes during the past 300 years: a historical perspective. Int J Environ Res Public Health 13:847. https://doi.org/10.3390/ijerph13090847

Morice CP, Kennedy JJ, Rayner NA et al (2012) Quantifying uncertainties in global and regional temperature change using an ensemble of observational estimates: the HadCRUT4 data set. J Geophys Res: Atmos 117:D08101. https://doi.org/10.1029/2011JD017187

Najafi MR, Zwiers FW, Gillett NP (2015) Attribution of Arctic temperature change to greenhouse-gas and aerosol influences. Nat Clim Change 5:246–249. https://doi.org/10.1038/NCLIMATE2524

Ng S, Perron P (2005) A note on the selection of time series models. Oxf B Econ Stat 67:115–134. https://doi.org/10.1111/j.1468-0084.2005.00113.x

Portnyagin YI, Merzlyakov EG, Solovjova TV et al (2006) Long-term trends and year-to-year variability of mid-latitude mesosphere/lower thermosphere winds. J Atmos Sol Terr Phys 68:1890–1901. https://doi.org/10.1016/j.jastp.2006.04.004

Przybylak R, Wyszyński P (2020) Air temperature changes in the Arctic in the period 1951–2015 in the light of observational and reanalysis data. Theor Appl Climatol 139:75–94. https://doi.org/10.1007/s00704-019-02952-3

Ribes A, Planton S, Terray L (2013) Application of regularised optimal fingerprinting to attribution. Part I: method, properties and idealised analysis. Clim Dyn 41:2817–2836. https://doi.org/10.1007/s00382-013-1735-7

Screen JA, Francis JA (2016) Contribution of sea-ice loss to Arctic amplification is regulated by Pacific Ocean decadal variability. Nat Clim Change 6:856–860. https://doi.org/10.1038/NCLIMATE3011

Shepherd A, Ivins ER, Geruo A et al (2012) A reconciled estimate of ice-sheet mass balance. Science 338:1183–1189. https://doi.org/10.1126/science.1228102

Shimizu S, Hoyer PO, Hyvärinen A, Kerminen A (2006) A linear non-Gaussian acyclic model for causal discovery. J Mach Learn Res 7:2003–2030. https://doi.org/10.1007/s10883-006-0005-y

Shindell D, Faluvegi G (2009) Climate response to regional radiative forcing during the twentieth century. Nat Geosci 2:294–300. https://doi.org/10.1038/NGEO473

Sies H (1988) A new parameter for sex education. Nature 332:495–495

Smith DM, Screen JA, Deser C et al (2019) The Polar Amplification Model Intercomparison Project (PAMIP) contribution to CMIP6: investigating the causes and consequences of polar amplification. Geosci Model Dev 12:1139–1164. https://doi.org/10.5194/gmd-12-1139-2019

Stern DI, Kaufmann RK (2014) Anthropogenic and natural causes of climate change. Clim Change 122:257–269. https://doi.org/10.1007/s10584-013-1007-x

Stips A, Macias D, Coughlan C, Garcia-Gorriz E, Liang XS (2016) On the causal structure between CO_2 and global temperature. Sci Rep 6:21691. https://doi.org/10.1038/srep21691

Stroeve J, Notz D (2018) Changing state of Arctic sea ice across all seasons. Environ Res Lett 13:103001. https://doi.org/10.1088/1748-9326/aade56

Suo L, Otterå OH, Bentsen M, Gao Y, Johannessen OM (2013) External forcing of the early 20th century Arctic warming. Tellus A 65:187–190. https://doi.org/10.3402/tellusa.v65i0.20578

Svendsen L, Keenlyside N, Bethke I, Gao Y, Omrani NE (2018) Pacific contribution to the early twentieth-century warming in the Arctic. Nat Clim Change 8:793–797. https://doi.org/10.1038/s41558-018-0247-1

Tomé A, Miranda P (2005) Continuous partial trends and low-frequency oscillations of time series. Nonlinear Proc Geophys 12:451–460. https://doi.org/10.5194/npg-12-451-2005

Triacca U, Attanasio A, Pasini A (2013) Anthropogenic global warming hypothesis: testing its robustness by Granger causality analysis. Environmetrics 24:260–268. https://doi.org/10.1002/env.2210

Vannitsem S, Dalaiden Q, Goosse H (2019) Testing for dynamical dependence—application to the surface mass balance over Antarctica. Geophys Res Lett 46:12125–12135. https://doi.org/10.1029/2019GL084329

Vose RS, Arndt D, Banzon VF et al (2012) NOAA's merged land-ocean surface temperature analysis. B Am Meteorol Soc 93:1677–1685. https://doi.org/10.1175/BAMS-D-11-00241.1

Wu CJ, Krivova NA, Solanki SK et al (2018) Solar total and spectral irradiance reconstruction over the last 9000 years. Astron Astrophys 620:A120. https://doi.org/10.1051/0004-6361/201832956

Yang P, Wang G, Zhang F, Zhou X (2016) Causality of global warming seen from observations: a scale analysis of driving force of the surface air temperature time series in the Northern Hemisphere. Clim Dyn 46:3197–3204. https://doi.org/10.1007/s00382-015-2761-4